Magnetoelectric Effect in Graphene Nanoribbons on Substrates via Electric Bias Control of Exchange Splitting

Zhuhua Zhang,[1] Changfeng Chen,[2] and Wanlin Guo[1,*]

[1]*Institute of Nano Science, Nanjing University of Aeronautics and Astronautics, Nanjing 210016, China*

[2]*Department of Physics and High Pressure Science and Engineering Center, University of Nevada, Las Vegas, Nevada 89154, USA*

(Received 15 June 2009; revised manuscript received 14 September 2009; published 30 October 2009)

We predict a magnetoelectric (ME) effect in graphene nanoribbons on silicon substrates by first-principles calculations. It is shown that a bias voltage can produce strong linear ME effect by driving charge transfer between the nanoribbons and substrate, thus tuning the exchange splitting of magnetic edge states; moreover, the bias induced n-to-p-type transition in the ribbon layer can switch the ME coefficient from negative to positive due to the unique symmetry of band structures. This mechanism is proven to be robust against variations in material and physical configurations, thus opening a new avenue for ME coupling in metal-free magnet systems of practical importance.

DOI: 10.1103/PhysRevLett.103.187204 PACS numbers: 75.80.+q, 71.15.Mb, 73.20.−r, 81.05.Uw

Magnetoelectric (ME) effect is the phenomenon of inducing magnetization by means of an electric field or inducing polarization by means of a magnetic field [1,2]. Linear ME effect has special importance for practical applications, which provides a linear interplay between the induced magnetism **M** and external electric field **E** [3], or $\mu_0 M_i = \alpha_{ij} \sum E_j$, where α_{ij} is the linear ME coefficient and μ_0 the permeability of free space. α_{ij} can be nonzero only for materials without the center and time-reversal symmetries [4]. In the past decades, two mechanisms for the effect that from the direct coupling of magnetic and ferroelectric orders and from interface coupling effects have been established, respectively, for traditional single-phase [5] and composite ME materials [6]. Motivated by the significant technological potential [7] and facilitated by the rapid development in nanotechnology, ME researches have recently been undergoing a tremendous revival [3,8]. Recently, two new mechanisms for ME coupling are proposed: (1) In dielectric/ferromagnet heterostructures and ferromagnetic metal films [9,10], field induced charge accumulation is spin-polarized at the interface or surface due to spin-dependent screening effect, resulting in a linear ME effect; (2) in ferroelectric-insulator–ferromagnet multilayers [11], ferroelectric displacements at the interface change the interfacial bonding strength, offering sizable change in the interface magnetizations. Actually, the two new mechanisms can inherently come from the same origin of spin-dependent charge transfer between two adjacent insulator-ferromagnet interfaces. Since the ME effects in these materials are confined to the interface or surface, the relationship between the induced surface-interface magnetization and external field can also be expressed as [10,12],

$$\mu_o \Delta M = \alpha E, \tag{1}$$

where α represents the surface ME coefficient. However, both the traditional and newly proposed ME mechanisms are related to localized d orbitals in transition metals or related materials to date. To extend the applications of ME technology to metal-free magnets containing only sp states should be more attractive [13–15] because the correlation effects between these electron states are demonstrated crucial to the magnetic ordering. Graphene-based magnets [16] are particularly interesting in this context due to its excellent mechanical properties and tremendous technological advantage in device flexibility and miniaturization. Especially, zigzag edges of graphene have been considered as a prototype for designing graphene-based spintronics devices, where spontaneous magnetic ordering appears along the edges [17]. Although a number of magnetic devices [14,18,19] with diverse functions have been conceived around the graphene edges, a great challenge remains in finding avenues for realizing the fundamentally important ME effect in the newly emerged magnetic materials. Here, we exploit unique properties of graphene on substrates, especially their sensitive charge carrier response to bias electric field [20,21], and unveil for the first time strong linear ME coupling in zigzag graphene nanoribbons (Z-GNRs) on technologically most widely used silicon substrates with entirely new mechanism and facility for control.

The first-principles calculations are performed using the Vienna *Ab initio* Simulation Package (VASP) code [22]. Ultrasoft pseudopotentials for the core region and local spin density approximation for the exchange-correlation potential are used. A kinetic energy cutoff of 530 eV is used in the plane-wave expansion. The system models contain one or two Z-GNR layers in *AB* stacking on silicon substrates consisting of seven silicon monolayers in a 2×6 surface unit cell. The dangling bonds of silicon atoms of the bottom layer and carbon atoms at the GNR edges are uniformly terminated by hydrogen atoms. The positions of silicon atoms of the topmost six monolayers plus the entire GNR atoms under each applied bias voltage are relaxed by conjugate gradient method until the force on each atom is less than 0.02 eV/Å, which is enough for

convergent edge magnetization in Z-GNRs. We consider a vacuum region of 12.5 Å to avoid the interaction between two adjacent images. The two-dimensional Brillouin-zone integration is sampled by up to 12 special k-points for structural optimization. Three primitive unit cells of Z-GNRs are chosen to match the double Si(001) surface unit cell, with the GNRs initially stretched by about 3%. The external electric field is introduced by planar dipole layer method [23] as implemented in VASP.

The model system used here to demonstrate the ME coupling consists of two Z-GNR layers in AB stacking on silicon substrates. Following the standard convention [14], we denote a Z-GNR containing N zigzag atomic chains across its width as Z_N-GNR. To show the main picture concisely, we first take the Z_7-GNR shown in Fig. 1 as an example. A freestanding Z_7-GNR shows spin-polarized edge states, with the spin states antiparallel on carbon atoms of different sublattices, A and B shown in Fig. 1(a). When a bilayer Z_7-GNR is adsorbed on a Si(001) surface, the spin edge states disappear in the bottom GNR layer due to the formation of sp^3 bonds at the edges [24] but are retained on the top layer; see Fig. 1(b) here and Fig. S1 in the supplementary material [25] for details. The magnetization density on the top GNR layer is similar to that of a freestanding GNR because of the weak binding to the bottom layer at an average interlayer distance of 3.4 Å, close to the bulk graphite value of 3.35 Å. However, the system with a substrate is physically distinguished from a freestanding GNR layer due to the charge transfer from the bottom GNR layer to the top layer, as a result of lower electrostatic potential at the bottom GNR layer induced by bonding with the substrate. Thereby the top GNR layer is intrinsically n-doped, and the magnetic moment per edge carbon atom is reduced to $0.20\mu_B$ from the pristine value of $0.24\mu_B$ in the freestanding state. Similar spontaneous charge transfer has been experimentally observed in bilayer graphene on epitaxial Si-C [26,27]. Here, we focus on the average moment per carbon at the left ribbon edge as the values of magnetization magnitude on two ribbon edges of the top layer are essentially identical.

Since the magnetic moment of the top GNR layer can be sensitively influenced by spontaneous charge transfer from the bottom layer, we further apply a bias voltage to control the interlayer charge transfer which, in turn, modulates the edge moment. We define the electric field along the normal of the substrate surface as a positive bias as shown in the inset of Fig. 2. It is found that the amount of charge transferred to the top Z_7-GNR decreases linearly with decreasing bias field, leading to a n-to-p-type transition at a bias voltage around -0.3 V/Å, see Fig. 2. It is interesting that the edge moment decreases linearly with increasing bias field in the n-doped region, but increases linearly in the p-doped region, producing a carrier-tunable linear ME effect. As the ME modulation is confined only in the top GNR layer, we use the Eq. (1) to extract the coefficient α in the two linear regions. By fitting the calculated data, we obtain α (in units of 10^{-12} G cm^2/V) in the n- and p-doped regions to be $\alpha_n = -0.53$ and $\alpha_p = 0.26$, respectively. Contrary to the ME effect at the left ribbon edge, the ME coefficients at the right edge are calculated to be $\alpha_n = 0.51$ and $\alpha_p = -0.25$. These ME coefficients are up to tens of times higher than the surface ME coefficients obtained in recently discovered ferromagnetic metal films [10] and nearly in the same order as those at the interface of metal oxide heterostructures [9].

The origin of this strong ME coupling is shown in Fig. 3. Because the electronic states around E_F in the top GNR layer are from the localized edge states (see Fig. S1(a) in the supplementary material [25]), the field induced charge transfer has a significant influence on the electron filling of the edge states, as shown for the left edge in Fig. 3(a). In the n-doped region, increasing bias field increases the

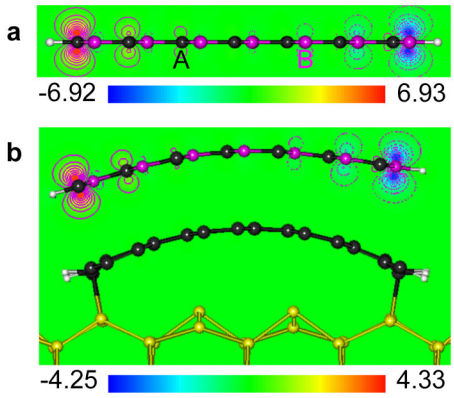

FIG. 1 (color online). Magnetization density (charge density of up-spin minus down-spin) for the ground state of a freestanding (a) and adsorbed bilayer (b) Z_7-GNRs on the Si(001) surface. The yellow (bright), black (dark), and white balls denote the silicon, carbon, and hydrogen atoms, respectively. The black and violet (grey) balls in the single or top layer GNR represent atomic sites belonging to the A and B sublattices, respectively. The contour spacing is set to be 80×10^{-3} e/Å^3.

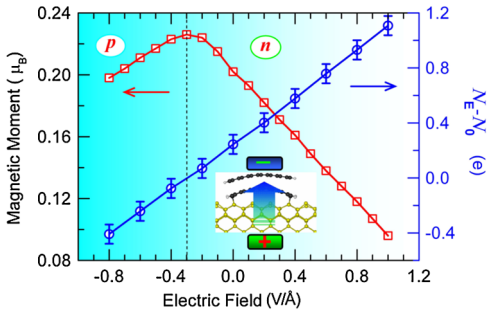

FIG. 2 (color online). Charge transfer induced ME effect in the adsorbed bilayer Z_7-GNR on Si(001) substrate. Blue line with circles: The amount of charge transferred to the top GNR layer as a function of electric field strength. N_E and N_0 present the total number of electrons in the top GNR layer under bias voltage and those in a neutral freestanding Z_7-GNR, respectively. Red line with squares: magnetic moment per edge carbon atom of A sublattice in the top layer as a function of the field strength.

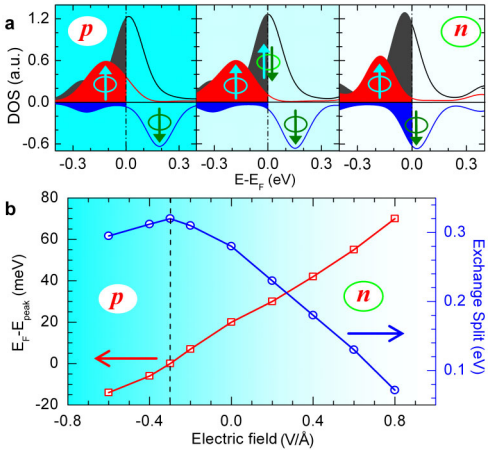

FIG. 3 (color online). Mechanism for the ME effect in the adsorbed bilayer Z_7-GNR. (a) Average local spin-up (↑), spin-down (↓) and spin-unresolved (dark grey line) DOS of the left edge carbon atom in the top Z_7-GNR layer under electric field strengths (left to right) -0.6, -0.3, and 0.4 V/Å. The occupied electronic states are marked in shadow. (b) Dependence of the peak position of the total localized DOS with respect to E_F and the exchange splitting of the left edge states of the top Z_7-GNR on the applied electric field.

electron filling and further moves the peak of the localized DOS downward below E_F, enhancing the n-type doping character [Fig. 3(a), right]. When spin-polarization is invoked, the up-spin and down-spin states form the valence band top and the conduction band bottom, respectively, at the left ribbon edge; see Fig. S1(c) in the supplementary material [25]. Extra electrons entering the left edge of the top layer will exclusively fill the down-spin states, while the up-spin states remain unchanged [Fig. 3(a), right]. As a result, the edge magnetization, which is proportional to the number of up-spin electrons minus down-spin electrons ($N_\uparrow$-$N_\downarrow$), is reduced with increasing bias voltage, leading to a negative ME coefficient. In contrary, in the p-doped region, the depopulated electrons in the top layer are mainly from the up-spin states due to the symmetry of the spin-polarized bands. So the edge magnetization is still reduced with bias voltage, but the ME coefficient becomes positive considering the change of field direction [Fig. 3(a), left]. Nevertheless, the magnitude of α_p is smaller than that of α_n. This is because at the left ribbon edge, the down-spin states have notable distribution of electronic states below E_F, leading to smaller spin-polarization at E_F in the p-doped region, and meanwhile the up-spin states are remarkably more delocalized than the down-spin states as evidenced by its larger dispersion shown in Fig. S1(c) of the supplementary material [25]. Similar mechanism inducing reverse ME effects can be found at the right ribbon edge (see Fig. S2 of the supplementary material [25]). This interesting ME effect can be further illustrated by the decrease in exchange splitting of the edge states, which is measured by the energy interval between the DOS peaks of the up- and down-spin states, with increasing bias voltage in the n-doped region, but an increase in the p-doped region, as shown in Fig. 3(b). At the neutral state shown in Fig. 3(a), the total DOS is just peaked at E_F with maximized exchange splitting and thus maximum edge magnetization as determined by the Stoner criterion [28].

Physically, this carrier-tunable linear ME effect arises from an entirely new mechanism: Charge carrier doping into the top GNR driven by bias fields controls the exchange splitting of the localized edge states, and the n-to-p transition changes the sign of ME coefficients. This is in contrast to the conventional ME behavior in single-phase materials which is due to field induced displacement of ions modifying the magnetic exchange interactions [7] or the mechanisms in metal films or oxide multilayer that arise from spin-dependent screening of the electric field [9–11]. To be more clarified, we remove the nonmagnetic bottom GNR layer and substrate from the system and keep the top GNR layer fixed, then recalculate the change of edge moment with bias voltage. We find that the ME modulation nearly disappears, indicating that spin-dependent screening plays a negligible role for the ME response of our system. On the other hand, while applying transverse electric field to a freestanding Z-GNR can also modulate the edge moment [14], it can only be realized under high fields, at which the GNR is close to a half-metal. Moreover, the half-metallic behavior can be maintained only within a finite range of electric field and can be completely removed by the nonlocal exchange interaction in Z-GNRs [29], in contrast to consistent ME modulation in our system over the entire field strengths.

We also examine the dependence of the ME effect on substrate thickness. Figure 4(a) shows that the ME coefficient is larger for thicker substrates. This result has important implication for ME modulation in practical applications because actual substrate size can reach up to

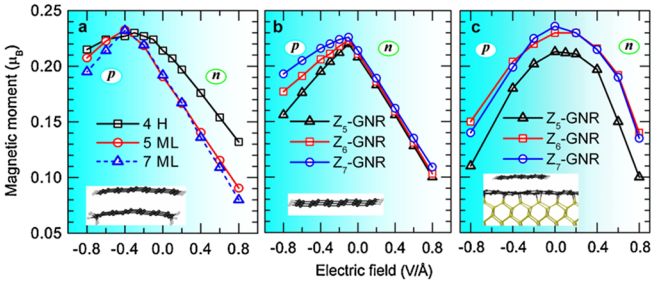

FIG. 4 (color online). Robustness of the ME effect. (a) ME effect in bilayer Z_6-GNR on Si(001) substrates with different thicknesses. Inset shows the configuration of the bilayer GNR with 4 hydrogen atoms binding to the bottom layer edges and all the silicon layers being removed, denoted as case 4 H. ML denotes the number of silicon monolayers of the substrate. $\alpha_n \approx -0.49$, -0.63, and -0.66 for the 4 H, 5 ML, and 7 ML cases, respectively. (b) Edge magnetic moment of freestanding Z-GNRs changes with equivalent field strength by charge injection (see text). Equivalent $\alpha_n \approx 0.68$, 0.67, and 0.65 for the Z_{5^-}, Z_{6^-}, and Z_7-GNRs, respectively. (c) ME effect in Z_{5^-}, Z_{6^-}, and Z_7-GNR layers over a 2D graphene layer adsorbed on Si(001).

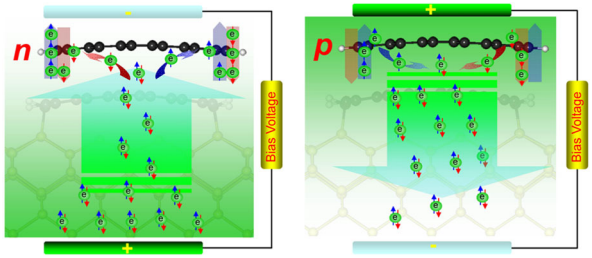

FIG. 5 (color online). Schematic illustration for the bias voltage induced ME effect in n- and p- (right panel) doped Z-GNRs. Short arrows denote the spin directions of the electrons.

several hundred nanometers. On the other hand, even when the substrate is totally removed with all Si-C bonds replaced by C-H bonds, the calculated α_n is still up to -0.49 for the top Z_6-GNR layer. This indicates that physical support of the substrate is not essential for the ME effect, providing existence of charge injection into the top magnetic layer. To be more substantiated, we further examine the moment modulation in freestanding single-layer Z-GNRs by charge injection, with a uniform positive jellium countercharge, as shown in Fig. 4(b). When we convert the injected charge into *equivalent* electric field according to the linear relationship shown in Fig. 2 between extra charge carrier on the top GNR layer and applied electric field, it is interesting that the single-layer Z-GNRs still show the similar linear ME effect. The *equivalent* ME coefficient is nearly independent of ribbon width in the n-doped region, but remarkably decreases with increasing ribbon width in the p-doped region at the left ribbon edge, see Fig. 4(b). This is because the valence band top becomes more localized in narrower Z-GNR due to stronger overlap between the two opposite edge states.

Our extensive calculations also show robustness of the ME effect to variations in material configurations and physical conditions. Even a single-layer Z-GNR over a 2D graphene sheet fully adsorbed on the Si(001) substrate also exhibits remarkable quasilinear ME effect under applied bias voltage [Fig. 4(c)], with the ME coefficient nearly independent of the ribbon width. The ME effect is also found to be robust to change in interlayer spacing, stacking, and location of the formed sp^3 bonds between the bottom GNR layer and the substrate, and can exist in a single-layer Z-GNR on H-terminated Si(001) and bilayer Z-GNR on clean Si(111) substrate as well (see Figs. S3–S5 in the supplementary material [25]).

We finally schematically summarize the mechanism for the distinguished ME effect in Fig. 5. Once the charge carriers are transferred by bias into the top GNR layer, the unique symmetry of band structure in the Z-GNRs determines that only one spin channel can be filled under a given bias at each ribbon edge, with the spin direction dependent on the type of carriers, leading to a carrier-tunable linear change in the edge magnetization with the bias field that is robust to variations in the buffer carbon layer and substrate configurations. The process promises an extremely high facility in ME modulation due to small spin-orbit and hyperfine interaction in carbon [30]. The predicted ME effect raised by the mechanism shown in Fig. 5 should not be unique to graphene nanoribbons, but may also be extrapolated to all monolayer molecules with magnetism survived on any solid substrates, providing that the charge can be driven by bias electric field into the magnetic layers.

This work was supported by the 973 Program (No. 2007CB936204), National NSF (No. 10732040), Jiangsu Province NSF (BK2008042), and the Ministry of Education (IRT0534) of China. Work at UNLV was supported by the US Department of Energy under Cooperative Agreement (No. DE-FC52-06NA26274).

*wlguo@nuaa.edu.cn

[1] J. Rondinelli *et al.*, Nature Nanotech. **3**, 46 (2008).
[2] W. Eerenstein *et al.*, Nature (London) **442**, 759 (2006).
[3] M. Fiebig, J. Phys. D **38**, R123 (2005).
[4] L. D. Landau and E. M. Lifschitz, *Electrodynamics of Continuous Media* (Oxford, Pergamon, 1960).
[5] I. Dzyaloshinskii, Sov. Phys. JETP **10**, 628629 (1960).
[6] G. Srinivasan *et al.*, Phys. Rev. B **64**, 214408 (2001).
[7] C. Binek and B. Doudin, J. Phys. Condens. Matter **17**, L39 (2005).
[8] N. A. Spaldin and M. Fiebig, Science **309**, 391 (2005).
[9] J. Rondinelli *et al.*, Nature Nanotech. **3**, 46 (2008).
[10] C. G. Duan *et al.*, Phys. Rev. Lett. **101**, 137201 (2008).
[11] C. G. Duan *et al.*, Phys. Rev. Lett. **97**, 047201 (2006).
[12] C. G. Duan *et al.*, Phys. Rev. B **79**, 140403(R) (2009).
[13] T. L. Makarova *et al.*, Nature (London) **413**, 716 (2001).
[14] Y. W. Son *et al.*, Nature (London) **444**, 347 (2006).
[15] H. Pardo *et al.*, arXiv:cond-mat/0407303v1.
[16] Y. Wang *et al.*, Nano Lett. **9**, 220 (2009).
[17] S. Okada and A. Oshiyama, Phys. Rev. Lett. **87**, 146803 (2001).
[18] W. Y. Kim and K. S. Kim, Nature Nanotech. **3**, 408 (2008).
[19] F. Munoz-Rojas *et al.*, Phys. Rev. Lett. **102**, 136810 (2009).
[20] T. Ohta *et al.*, Science **313**, 951 (2006).
[21] F. Wang *et al.*, Science **320**, 206 (2008).
[22] G. Kresse and J. Furthmuller, Phys. Rev. B **54**, 11169 (1996).
[23] J. Neugebauer and M. Scheffler, Phys. Rev. B **46**, 16067 (1992).
[24] Z. Zhang and W. Guo, Appl. Phys. Lett. **95**, 023107 (2009).
[25] See EPAPS Document No. E-PRLTAO-103-020946 for supplementary analysis and discussion details. For more information on EPAPS, see http://www.aip.org/pubservs/epaps.html.
[26] A. Bostwick *et al.*, Nature Phys. **3**, 36 (2007).
[27] S. Y. Zhou *et al.*, Nature Mater. **6**, 770 (2007).
[28] D. M. Edwards and M. I. Katsnelson, J. Phys. Condens. Matter **18**, 7209 (2006).
[29] E. Rudberg *et al.*, Nano Lett. **7**, 2211 (2007).
[30] B. Trauzettel *et al.*, Nature Phys. **3**, 192 (2007).